J. Fluid Mech. (2009), *vol.* 618, *pp.* 135–154.
doi:10.1017/S0022112008004102 Printed in the United Kingdom

Electromagnetic control of thermal convection of a fluid with strongly temperature-dependent material properties

CORNELIA GIESSLER AND ANDRÉ THESS†

Department of Mechanical Engineering, Ilmenau University of Technology, P.O. Box 100565, 98684 Ilmenau, Germany

(Received 27 September 2007 and in revised form 24 August 2008)

We study a one-dimensional model describing buoyancy-driven laminar steady flow of a glass melt in a closed loop under the influence of a localized electromagnetic (Lorentz) force. The loop is a highly simplified representation of a closed streamline in glass melt flow in a real furnace under the influence of an artificially produced Lorentz force. The model is based on the energy equation for the temperature and the Stokes equation for the velocity distribution inside the loop. We take into account the full nonlinear temperature dependence of the viscosity and the electrical conductivity of the melt. The three-dimensional problem is then reduced to a single nonlinear equation for the cross-section averaged velocity from which the one-dimensional temperature distribution along the loop can be readily obtained. We show that the two-way interaction between the velocity and temperature resulting from the temperature-dependent material properties and Lorentz force leads to the result that the mean velocity as a function of the control parameters is non-unique and involves bifurcations. For some parameters we even observe freezing, which refers to a regime in which the fluid is almost at rest. Our model reveals the role of temperature-dependent viscosity and conductivity in glass melt flows in a pure form that is not visible in full numerical simulations.

1. Introduction

Nowadays it is common to use mechanical stirrers or electric boosters to increase convection in glass melting furnaces so as to enhance the mixing efficiency. Recently, a novel approach to mixing enhancement, namely the simultaneous application of electric currents and external magnetic fields with the purpose to create Lorentz forces directly in the melt, has attracted attention (Osmanis, Snijedze & Aglitis 1987; Hofmann & Thess 2002; Kunert *et al.* 2004). Experimental results (Hülsenberg *et al.* 2004) have demonstrated that these additional Lorentz forces can influence the glass melt flow significantly and increase the homogenization. Numerical studies such as those of Giessler & Thess (in press) reveal the influence of the Lorentz force on the flow structure. However, such three-dimensional computations require long simulation times and are restricted to a limited number of parameters. Moreover, they fail to reveal the difference between the role of temperature-dependent viscosity and temperature-dependent electrical conductivity.

† Email address for correspondence: thess@tu-ilmenau.de

One possibility to perform extensive parameter studies and to obtain a deeper understanding of the basic physics is to develop simplified models that can be studied at low computational cost. The formulation of such a model is the goal of the present paper. The large convection rolls which arise in the melting furnace due to the high viscosity of the glass melt suggest to formulate such models on the basis of the assumption that the fluid is confined to an annular loop which contains heating, cooling and forcing zones. Such assumption enables us to study a one-dimensional form of the fluid flow and obtain a better understanding of the flow behaviour in a convection roll under the influence of external Lorentz forces.

More specifically, our present work is inspired by previous studies on natural circulation loops, also called thermosyphons, which consist of at least one heat source and one higher elevated heat sink connected by pipes. The convection in such loops is driven by buoyancy. These systems have various important applications in energy conservation systems, for example solar heaters and cooling systems of nuclear reactors, and have been the subject of a large number of theoretical and experimental studies. Reviews of the wide applications are given in Zvirin (1981) and Greif (1988). This field of research was pioneered by Keller (1966) and Welander (1967) who used natural circulation loops to model geothermal and geophysical processes. The Lorentz-like chaotic alternations of flow directions were also experimentally observed and theoretically analysed for example by Creveling *et al.* (1975) and Ehrhard & Müller (1990). Besides the most common analytical approach to average the governing equations over the pipe cross-section, Desrayaud, Fichera & Marcoux (2006) performed a two-dimensional time-dependent analysis showing the influence of radial components on the flow characteristic. In a few works, the fluid of the loop was considered to be electrically conducting. In the presence of a transverse magnetic field, eddy currents and a Lorentz force can be induced and can lead to a damping of the motion. The study in Poddubnaya & Shaidurov (1969), performed for two hydrodynamically connected vertical pipes heated from below, showed that the onset of convection is a function of the magnetic flux density. Ghaddar (1998*a*, *b*) studied the influence of the magnetic field density on the flow characteristic for similar geometries over a wide range of parameters.

To our knowledge, no studies about the influence of temperature-dependent material properties on the flow characteristics in a thermosyphon exist in the literature. Several analytical models describing the laminar flow of magma (e.g. Ockendon & Ockendon 1977; Helfrich 1995; Wylie & Lister 1995; Morris 1996) glass melt (e.g. Lange & Loch 2002; Giessler, Lange & Thess 2007) and polymers (e.g. Richardson 1986) revealed that the temperature-dependent viscosity modifies the flow significantly. The viscosity variations can lead to steady nonlinear flow characteristics, instabilities and multiple-valued solutions even in simple geometries like channels or pipes. Apart from the analytical approaches there have been experimental and numerical investigations of Rayleigh–Bénard convection cells with large viscosity variations which have been motivated by Earth's mantle convection. Already the pioneering works of Torrance & Turcotte (1971) and Booker (1976) followed by experiments of Richter, Nataf & Daly (1983) and analyses of Morris & Canright (1984) and Fowler (1985) show the modification of the spatial flow structures, heat transfer and transitional regimes due to the temperature-dependent viscosity. For extremely large viscosity variations a cold stagnant lid occupies most of the cold top boundary layer. Almost isoviscous convection occurs beneath the stagnant lid. The studies on the transitional regimes were numerically continued by Ogawa, Schubert & Zebib (1991) for a three-dimensional configuration and have been extended for a wide

range of Rayleigh numbers and viscosity contrast up to 10^{14} for a two-dimensional square cell by Moresi & Solomatov (1995). The mentioned works about forced convection in channels or pipes and free convection in bottom-heated cells show that the investigation of the flow of a fluid with temperature-dependent viscosity in a loop, even without Lorentz forces, represents a useful extension of natural circulation loops.

The present work is a direct continuation of our previous paper (Giessler *et al.* 2005) which dealt with an analytical model for a circular loop including a Lorentz force as an additional parameter. This model, like the present one, was motivated by the convection of glass melt in a crucible under the influence of external Lorentz forces. The Lorentz force in our previous work was generated by an electric current injected directly into the melt and a perpendicularly acting magnetic field density, whereby both fields were assumed to be independent of the flow in the loop. The fluid in the loop was considered to be driven by strongly localized heating and cooling sections. For a wide range of conditions, instabilities were found which led to multiple-valued solutions. Furthermore, this model, in spite of its simplicity, revealed the significant influence of the Lorentz force on the flow. However, this model did not include some key attributes of convection rolls in glass melts, namely (i) the strong dependence of viscosity and electrical conductivity on the temperature which, in practice, can lead to variations by more than one order of magnitude; (ii) the non-circular shape of the convection rolls (cf. the experiments by Hülsenberg *et al.* 2006 and the numerical simulations of Giessler & Thess in press); and (iii) the absence of isothermal regions in convection rolls.

We now focus on the mentioned characteristics (i)–(iii) for convection rolls of glass melt and present a new model for the highly viscous fluid in a closed loop. Besides the external Lorentz force we will study the influence of the variation of electrical conductivity and viscosity on the flow. We will show how the geometrical features of the loop – ranging from two hydrodynamically connected vertical branches to almost circular loops – can modify the flow as well. The definition of our model shall be described in § 2. The results are studied in § 3. We will discuss separately the role of Lorentz force, temperature-dependent electrical conductivity and temperature-dependent viscosity. Finally, we summarize the key results of this work and give some concluding remarks in § 4.

2. Formulation of the problem

We consider a tube of circular cross-section with the uniform radius R and the length $L \gg R$ bent to a closed loop with two vertical branches of length l. The two branches are connected by two circular arcs whose radius of curvature is denoted by r as shown in figure 1(*a*). We define the coordinate $s \in [0, L]$ with $L = 2l + 2\pi r$ as the arclength along the loop starting at the bottom of the right vertical branch. The variability of the aspect ratio r/l enables us to study loops of different shapes including the limiting cases of two hydraulically connected vertical branches ($r \to 0$ and $l \to L/2$, see figure 1*b*) as well as a circular loop ($l \to 0$ and $r \to L/2\pi$, see figure 1*c*).

The loop is filled with a viscous fluid with constant heat capacity c_P representing molten glass. We invoke the generalized Boussinesq approximation and assume that the density of the fluid is constant in all governing equations except for the buoyancy term in the Navier–Stokes equation. Here it is assumed to depend linearly on temperature and to obey $\rho = \rho_0(1-\beta\theta)$, with β representing the expansion coefficient, the temperature, and ρ_0 being the density for $\theta = 0$, $\theta > 0$. This linearized equation of state is a good approximation for glass melts. Our temperature scale is defined in

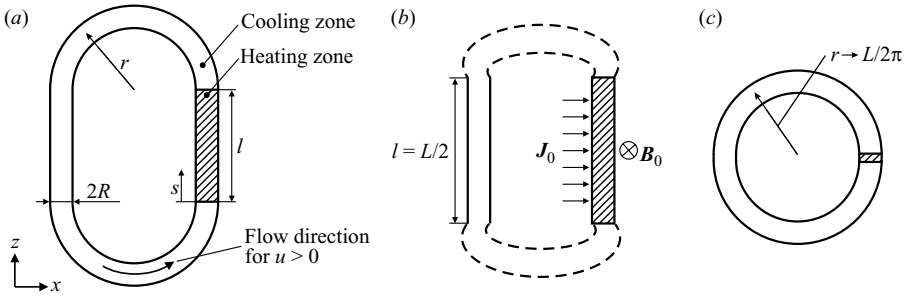

FIGURE 1. Sketch of the considered problem for (*a*) a loop with two vertical branches of the length l connected by two circular arcs with the arc radius r, (*b*) two hydrodynamically connected vertical branches corresponding to the limit $r \to 0$ and (*c*) a circular loop corresponding to the limit $l \to 0$. The dashed lines in (*b*) indicate the connection between the two vertical parts by sections with zero hydraulic resistance.

such a way that its zero corresponds to the freezing temperature of the glass melt under consideration. Although glass melts do not have a clearly defined freezing point, the motivation for our choice $\theta = 0$ as the freezing temperature will become clear shortly. We parenthetically note that we use the term generalized Boussinesq approximation in order to distinguish the present model which involves temperature-dependent viscosity and electrical conductivity (to be discussed below) from the usual meaning of the term Boussinesq approximation which implies that density is the only temperature-dependent property.

Glass melt is characterized by highly nonlinear temperature-dependent viscosity $\eta(\theta)$ and electrical conductivity $\sigma(\theta)$, where $\eta(\theta)$ is decreasing and $\sigma(\theta)$ is increasing with temperature. In glass science and engineering it is common to express these material parameters as exponential functions of temperature proportional to $\exp(1/\theta)$ (Vogel 1992). But other functions like for instance power laws fit the material property data equally well. Hence, we are free to choose the functional form of $\eta(\theta)$ and $\sigma(\theta)$ such that our analysis becomes most convenient. For reasons given below we use

$$\eta(\theta) = \eta_0 \left(\frac{\theta}{\theta_i}\right)^m, \quad m \leqslant 0, \tag{2.1}$$

with the viscosity parameters η_0 and m depending on the glass type. The normalization factor θ_i is set to 1 K to assure that η_0, which does not have a physical meaning, is measured in units of the viscosity. Since $\eta \to \infty$ for $\theta \to 0$ it becomes clear that the temperature $\theta = 0$ can be regarded as the freezing temperature of the melt. Hence, the viscosity law (2.1) only makes sense for $\theta > 0$. We further assume

$$\sigma(\theta) = \sigma_0 \left(\frac{\theta}{\theta_i}\right)^n, \quad n \geqslant 0, \tag{2.2}$$

again with constant parameters σ_0 and n specific to the considered glass melt. For $m = n = 0$ the fluid has a constant viscosity, $\eta = \eta_0$, and a constant electrical conductivity, $\sigma = \sigma_0$, respectively. The advantage of our power laws is their convenient algebraic handling when integrations are necessary. By contrast, the more common models involving the temperature dependence $\exp(1/\theta)$ do not yield to an analytic integration.

On the right vertical branch of the loop, $0 \leqslant s \leqslant l$, a constant electric current density $\boldsymbol{J}_0 = J_0 \boldsymbol{e}_x$ is applied and leads to a volumetric heat production according to

J_0^2/σ. This part of the loop is referred to as the heating zone. In the remaining part of the loop, $l \leqslant s \leqslant L$, a constant heat transfer coefficient h is prescribed at the pipe walls. Therefore, this branch is named cooling zone. The resulting temperature gradient along s leads to buoyancy-driven convection in a counterclockwise direction. We further assume that a time-independent external magnetic flux density $\boldsymbol{B}_0 = B_0 \boldsymbol{e}_y$, which is acting perpendicular to $\boldsymbol{J}_0$ in the right vertical branch, leads to a Lorentz force density $f_L = J_0 B_0 \boldsymbol{e}_z$ in the melt. Depending on the direction of $\boldsymbol{B}_0$, the Lorentz force either reinforces or counteracts the thermal convection. The Hartmann number which characterizes the ratio between the induced electromagnetic forces and the friction force (Davidson 2001) is assumed to be very small throughout the paper. Then the induced current density is negligible in comparison to the applied current density. Furthermore, we assume a low Brinkman number describing the relation between viscous heating and fluid conduction. This assumption enables us to neglect the effects of viscous dissipation on the energy balance.

The aim of this work is to derive a simplified model that predicts the cross-section averaged velocity u and the cross-section averaged temperature distribution $\theta(s)$ in the loop. Since we assume that our glass melt is incompressible, u does not depend on s. By virtue of our assumption $L \gg R$, the one-dimensional model of the flow and heat transfer to be derived below is expected to be sufficiently accurate, similar to previous works, e.g. Welander (1967) and Ehrhard & Müller (1990).

In general, the steady low-Reynolds-number flow at hand is governed by the three-dimensional Stokes equation including Lorentz force and the three-dimensional energy equation. For $L \gg R$, however, these equations can be reduced to a mathematical model that contains the coordinate s only. Since this approach has been extensively used in the past, we will not present the full derivation of the model here and refer the interested reader to the references Welander (1967), Ehrhard & Müller (1990), Giessler *et al.* (2005) and Giessler *et al.* (2007). The tangential component of the stationary cross-section averaged Stokes equation

$$\frac{\mathrm{d}p}{\mathrm{d}s} = (f_v + f_b + f_L) \cdot \boldsymbol{e}_s \tag{2.3}$$

is the relevant source of information to derive our model. This equation expresses the balance between the viscous f_v, buoyancy f_b and Lorentz f_L force densities on the one hand and the pressure gradient $\mathrm{d}p/\mathrm{d}s$ on the other hand. $\boldsymbol{e}_s$ is the unit vector tangential to the loop. Assuming a Poiseuille velocity profile, the viscous friction force becomes $f_v = -8u\eta(\theta(s))/R^2 \boldsymbol{e}_s$. The buoyancy force is given by the equation $f_b = \rho_0 \beta g \theta(s) \boldsymbol{e}_z$, where g denotes the acceleration of gravity. The Lorentz force acts only within the heating zone ($0 \leqslant s \leqslant l$) and reads $f_L = J_0 B_o \boldsymbol{e}_z$. To eliminate the pressure we integrate (2.3) from $s = 0$ to $s = L$. Making use of the uniqueness of the pressure expressed by $p(s + L) = p(s)$ we obtain

$$\frac{8u}{R^2} \int_0^L \eta(\theta(s))\, \mathrm{d}s = \rho_0 \beta g \int_0^L \theta(s) \boldsymbol{e}_z \cdot \boldsymbol{e}_s \, \mathrm{d}s + J_0 B_0 l. \tag{2.4}$$

Equation (2.4) expresses the balance between the integrated viscous friction on the left-hand side and the driving buoyancy and Lorentz forces on the right-hand side. The integrated buoyancy term has to be evaluated separately for each branch as buoyancy acts along the gravitational field in $\boldsymbol{e}_z$-direction. In detail the buoyancy

term takes the form

$$\int_0^L \theta(s)\boldsymbol{e}_z \cdot \boldsymbol{e}_s \,\mathrm{d}s = \int_0^l \theta(s)\,\mathrm{d}s + \int_l^{l+\pi r} \theta(s)\cos\left(\frac{s-l}{r}\right)\mathrm{d}s - \int_{l+\pi r}^{2l+\pi r} \theta(s)\,\mathrm{d}s - \int_{2l+\pi r}^{L} \theta(s)\cos\left(\frac{s-(2l+\pi r)}{r}\right)\mathrm{d}s.$$

To derive an equation for the one-dimensional temperature distribution $\theta(s)$ the heating and cooling zones have to be considered separately. In the heating zone there is no heat loss to the environment. Instead the increase of the heat flux carried by the mean flow is equal to the volumetric heating due to the Joule effect. Neglecting effects of heat diffusion, the steady-state energy equation for the heating zone is thus

$$\rho_0 c_P u \frac{\mathrm{d}\theta}{\mathrm{d}s} = \frac{J_0^2}{\sigma(\theta)} \quad \text{for } s \in [0, l]. \tag{2.5}$$

In the cooling zone the decrease of the heat flux carried by the mean flow is equal to the heat loss through the sidewall. This is expressed by the differential equation

$$\rho_0 c_P u \frac{\mathrm{d}\theta}{\mathrm{d}s} = -\frac{2h}{R}(\theta - \theta_\infty) \quad \text{for } s \in [l, L], \tag{2.6}$$

where θ_∞ represents the ambient temperature and h being the heat transfer coefficient. In the present work we set $\theta_\infty = 0$ to keep the model as simple as possible. With this simplification our model is a good approximation for the behaviour of a streamline which passes through the immediate vicinity of a (cold) outer wall of a melting crucible which involves strong cooling. However, the present analysis can be generalized to non-zero values of θ_∞. Such a model would be appropriate to describe the behaviour of an internal streamline with weak heat transfer. But non-zero values of θ_∞ would restrict us to a numerical treatment of the basic equations (2.4)–(2.6) instead of an algebraic solution which is one goal of the present work and reachable with $\theta_\infty = 0$.

To match the first-order differential equations (2.5) and (2.6) the condition of continuity between the cooling and heating zones at $s = 0$ and $s = l$ has to be fulfilled for θ. Once these equations have been solved for $\theta(s)$ we are able to evaluate the integrals in the Stokes equation (2.4), which then becomes an algebraic equation to determine u.

We non-dimensionalize the governing equations (2.4)–(2.6) using the loop length L as a measure for all geometric parameters, i.e.

$$s = s'L, r = r'L, l = l'L \text{ and } R = R'L.$$

Furthermore, we use the following scales for the velocity u and temperature θ:

$$u = u'u_0, \text{ with } u_0 = \frac{8\eta_0 L}{R^2\rho_0} \text{ and } \theta = \theta'\theta_0, \text{ with } \theta_0 = \left(\frac{J_0^2 R^2 \theta_i^n}{8\eta_0\sigma_0 c_P}\right)^{1/(1+n)}.$$

After substituting these definitions in (2.4)–(2.6) and dropping the primes, we obtain the Stokes equation in the form

$$u\int_0^1 \theta^m(s)\,\mathrm{d}s = Gr\int_0^1 \theta(s)\boldsymbol{e}_z \cdot \boldsymbol{e}_s \mathrm{d}s + M, \tag{2.7}$$

where

$$Gr = \frac{\beta g \rho_0^2 R^4 \theta_0}{64\eta_0^2 L}\left(\frac{\theta_0}{\theta_i}\right)^{-m} \tag{2.8}$$

is the modified Grashof number which represents the ratio of the square of the viscous diffusion time scale to the square of the free-fall velocity time scale. Moreover,

$$M = \frac{J_0 B_0 l R^4 \rho_0}{64 \eta_0^2 L^2} \left(\frac{\theta_0}{\theta_i}\right)^{-m} \tag{2.9}$$

is the modified interaction parameter which can be regarded as the ratio of the Lorentz force to the viscose force. Let us stress that Gr and M already include the dependence of viscosity and electrical conductivity on temperature as these parameters are proportional to $(\theta_0/\theta_i)^{-m}$. The non-dimensional energy equation for the heating zone becomes simply

$$u \frac{\mathrm{d}\theta}{\mathrm{d}s} = \theta^{-n}, \tag{2.10}$$

and the energy equation for the cooling zone becomes

$$u \frac{\mathrm{d}\theta}{\mathrm{d}s} = -N\theta, \tag{2.11}$$

where

$$N = \frac{hR}{4\eta_0 c_P} \tag{2.12}$$

is the wall heat loss parameter of the cooling zone. The integration of the non-dimensional energy equations (2.10) and (2.11) gives the solution for the temperature distribution

$$\theta(s) = \left[(g \exp \varepsilon)^{n+1} + \frac{n+1}{u} s\right]^{1/(n+1)} \quad \text{for } s \in [0, l], \tag{2.13}$$

$$\theta(s) = g \exp\left\{-\frac{N}{u}(s-l)\right\} \quad \text{for } s \in [l, 1], \tag{2.14}$$

with

$$\epsilon = -\frac{N}{u}(2\pi r + l), \; g = \left\{\frac{l(n+1)}{u(1-(\exp \epsilon)^{n+1})}\right\}^{1/(n+1)}.$$

The substitution of (2.13) and (2.14) in (2.7) leads, after some elementary calculations, to the following algebraic form of the momentum equation

$$\begin{aligned} u g^m & \left\{\frac{n+1}{n+m+1} l \frac{1-(\exp \epsilon)^{n+m+1}}{1-(\exp \epsilon)^{n+1}} + \frac{u}{mN}\left[1-(\exp \epsilon)^m\right]\right\} \\ & = Gr\, g \left\{\frac{Nr^2/u}{(Nr/u)^2+1}\left[1+\exp \epsilon_1 - \exp \epsilon_2 - \exp \epsilon\right] + \frac{u}{N}\left[\exp \epsilon_2 - \exp \epsilon_1\right]\right. \\ & \quad \left. + \frac{n+1}{n+2} l \frac{1-(\exp \epsilon)^{n+2}}{1-(\exp \epsilon)^{n+1}}\right\} + M, \end{aligned} \tag{2.15}$$

with $\epsilon_1 = \exp(-Nr\pi/u)$ and $\epsilon_2 = \exp(-N(r\pi + l)/u))$. Equation (2.15) expresses the balance between the braking friction force on the left-hand side and the buoyancy and Lorentz forces on the right-hand side. As $Gr \geqslant 0$, the buoyancy force drives the fluid always into a counterclockwise direction which corresponds to $u > 0$. The interaction parameter M can have both positive or negative sign. Therefore, the Lorentz force reinforces buoyancy for $M > 0$ with $u > 0$ or counteracts the buoyancy when $M < 0$. The algebraic equation (2.15) is our desired model which we can use to calculate the velocity u as function of the modified Grashof number Gr, the interaction parameter

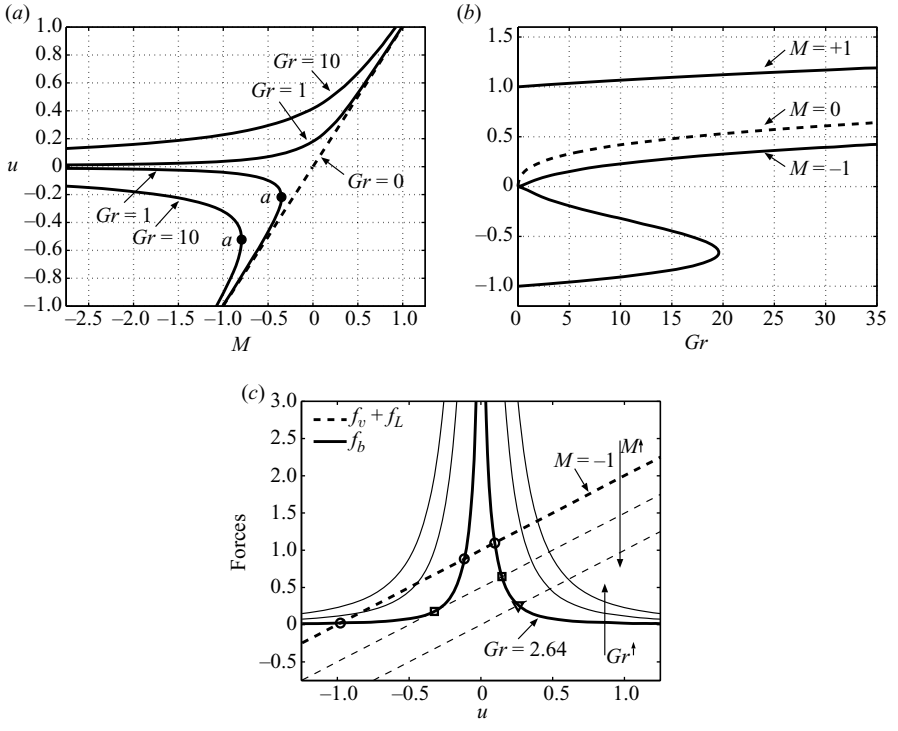

FIGURE 2. Influence of the Lorentz force on a system with constant material properties ($n = m = 0$) and $l = 0.25$: the mean velocity u is plotted (a) as a function of the interaction parameter M for different Grashof numbers Gr and (b) as a function of Gr. (c) The intersection points of the buoyancy force f_b and the Lorentz and friction force ($f_v + f_L$) give the solution of our governing equation (2.15) for $Gr = 2.64, 15, 30$ and $M = -1, -0.5, 0$. Depending on M we have one (∇), two ($\square$) or three ($\bigcirc$) intersection points and therefore one, two or three solutions for the velocity u for a given set of parameters. For $M = 0$ we have no Lorentz force and for $M > 0$ and $M < 0$ Lorentz force and buoyancy act in the same and in the opposite direction, respectively.

M, the cooling parameter N, the electrical conductivity parameter n, the viscosity parameter m and the aspect ratio r/l with $2\pi r + 2l = 1$.

The rest of the paper is devoted to the treatment of (2.15). We apply a simple root finding procedure on (2.15) to obtain u.

3. Results

The purpose of our investigation is to understand how buoyancy-driven flow of a fluid with constant material properties is modified if (i) a Lorentz force is applied and if (ii) the electrical conductivity and (iii) the viscosity become temperature-dependent. In practice all these three effects are present simultaneously. However, we believe that in order to develop a systematic understanding of the interplay of these effects, it is preferable to study first the effect of Lorentz force on a fluid with constant material properties and then investigate the effects of temperature-dependent conductivity and viscosity separately. This will be done next.

3.1. *Influence of Lorentz force on a system with constant material properties*

First we investigate a system with constant material properties, $n = m = 0$, and study the influence of the Lorentz force. In figure 2(a) the mean velocity u is given as

a function of the interaction parameter M for different Grashof numbers Gr. If we neglect buoyancy, $Gr = 0$, (2.15) reduces to $u = M$. This trivial solution which corresponds to electromagnetically driven flow of an isothermal fluid is shown by the dashed line in figure 2(a). The picture changes significantly if we 'switch on' buoyancy ($Gr > 0$), as was already found in Giessler *et al.* (2005) for a circular loop. Indeed, $u(M)$ is now a multiple-valued function for some values of the interaction parameter.

Let us first consider a system with positive velocities. (Remember that positive velocity corresponds to a flow in counterclockwise direction.) The key to the understanding of this phenomenon is the observation that for small positive velocities strong temperature gradients build up within the loop and lead to intensive buoyancy forces. In order to highlight this effect we plot the non-dimensional buoyancy force as a function of the velocity as a solid line in figure 2(c). This figure shows that f_b has a singularity for $u = 0$. The singularity of the buoyancy force for $u \to 0$ occurs for two reasons, namely neglect of heat conduction along the loop and the linearized density–temperature relationship used in the Boussinesq approximation. Indeed, since heat cannot be conducted in longitudinal direction and cannot escape from the insulated heating section, heat builds up without bound for $u \to 0$ which leads to $\theta \to 0$. If the exact relation $\rho(\theta)$ would have been used, ρ would tend to a small but finite value as $\theta \to \infty$ leaving the buoyancy force finite. Since we use the linearized relation $\rho = \rho_0(1 - \beta\theta)$, instead, $\rho \to \infty$ as $\theta \to \infty$ which gives rise to an infinite buoyancy force. Consequently, the behaviour of $u(Gr, M)$ in figure 2(a) should be considered as non-physical in the limit $M \to \infty$. If longitudinal heat conduction and non-Boussinesq effects were taken into account, the branches $u > 0$ and $u < 0$ for large negative M would be smoothly connected. Nevertheless, it is interesting to see that a Lorentz force counteracting the buoyancy force cannot easily stop the flow. The solution $u(M)$ of (2.15) shown in figure 2(a) can be graphically interpreted as the intersection of the curves f_b and $f_v + f_L$ as functions of u. As indicated in figure 2(c), an intensification of the counteracting Lorentz force ($M < 0$) leads to a shift of the intersection points along the right branch of f_b, but not to a change of the flow direction.

Let us now look at the regime with large and negative velocities which evolves from the dashed straight line in figure 2(a) for $M < 0$ if we switch on buoyancy. If we start from strong negative M and decrease the magnitude of this parameter, the magnitude of the mean velocity also decreases until the influence of buoyancy becomes relevant. For $u \to 0$ we find hot fluid just below and inside the heating zone and cold fluid in the cooling zone, hence a large buoyancy force builds up acting opposite to the flow direction. To obtain a stable system the driving Lorentz force has to increase very strongly. As a result, we find a turning point in $u(M)$ for $u < 0$, labelled as 'a' in figure 2(a). Altogether, for $Gr > 0$ the curve $u(M)$ splits into two branches: One the upper branch with $u > 0$, the velocity asymptotically reaches $u \to 0$ for $M \to -\infty$ and $u = M$ for $u \to \infty$. The lower branch with $u < 0$ runs from $u = M$ for $u \to -\infty$ over the turning point a to $u \to 0$ for $M \to -\infty$. For $M < M(a)$ three steady solutions for the velocity can be found for one set of parameters. The velocity as a function of Lorentz force was already studied in Giessler *et al.* (2005) for $u \geqslant 0$ and a circular loop. A comparison shows that the results of both models agree quantitatively. The physical behaviour is reproduced by both models. The results for negative velocities cannot be compared as this parameter range has not been studied in Giessler *et al.* (2005).

The multiple-valued character of u for $M < 0$ can also be observed if the mean velocity is plotted as a function of the Grashof number Gr as shown in figure 2(b). The curve for $M = -1$ develops two turning points and there exists a range of Gr numbers over which three steady states can be found. Between the two turning points

we observe a counterintuitive behaviour – the magnitude of the clockwise buoyancy force increases as well. On the upper branch we have $u > 0$ for all $Gr > 0$. On the lower branch we have $u < 0$ as the clockwise acting Lorentz force is the dominating driving force. Here the absolute value of the velocity decreases with Gr as buoyancy increases until the turning point is reached. If we incidentally increase Gr, buoyancy predominates $f_b > f_L + f_v$ and no equilibrium is reached (see e.g. figure 2*c*). The fluid slows down, buoyancy increases as the temperature gradient increases and leads to an amplification of the slow-down process. After the change of the flow direction buoyancy decreases with velocity until the balance between the forces is reached. This change of flow direction appears in $u(Gr)$ as a jump from the inflexion point of the lower branch with $u < 0$ to the upper branch with $u > 0$. The upper and the lower branches of the curve $u(Gr)$ are stable while the middle branch is unstable. This can be explained with reference to figure 2(*c*) as follows. Consider a state located on the downward sloping branch of the curve $u(Gr)$ for $M = 1$ which corresponds to clockwise motion. Let us assume that an external perturbation leads to slight shift of u in positive direction (i.e. from u to $u + du$ with $du > 0$) which corresponds to a weak 'kick' in counterclockwise direction. As the curve $f_b(u)$ in figure 2(*c*) shows, the buoyancy force will then change from f_b to $f_b + df_b$ with $f_b > 0$. This implies that the fluid will experience a force in positive (counterclockwise) direction which brakes the clockwise motion further. This closed-loop interaction reinforces the deviation of u from its initial state even further and signifies an unstable branch.

3.2. *Temperature-dependent electrical conductivity*

Now we turn our discussion to a circular loop, $2l \ll 1$, with temperature-dependent electrical conductivity, $n > 0$, and constant viscosity, $m = 0$. Figure 3(*a*) shows u as a function of M for $Gr = 10$ and various electrical conductivity parameters n. Let us first note that the dashed curve with $n = 0$ in figure 3(*a*) and the curve for $Gr = 10$ in figure 2(*a*) follow the same characteristics and pertain to similar physical situations. However, the numerical values of both curves are not identical. This quantitative difference originates from the reduction of the length of the heating zone from $l = 0.25$ ($Gr = 10$ in figure 2) to $l = 0.005$ ($n = 0$ in figure 3) which leads to a reduction of the heat input and, hence, to a reduction of buoyancy. As a result, the velocity becomes smaller in a buoyancy dominated regime (e.g. $M = 0$) and the turning point shifts to velocities with a smaller magnitude for the present system with $l = 0.005$.

Furthermore, figure 3(*a*) shows that the temperature-dependent electrical conductivity leads to a dramatic change of the flow characteristic $u(M)$. In the case $M < 0$ there are regions where there exist three solutions for u. Such a multiple-valued solution can also be found if we plot u as function of the Grashof number Gr as it is done in figure 3(*b*). If the Lorentz force acts against buoyancy, $M < 0$, and M reaches a certain critical value, there is a range of Grashof numbers over which three steady states can be found for positive velocities (see the curve with $M = -1$ in figure 3*b*). The curve develops two overturning points, which are labelled with a and b in figure 3(*b*). We note that between these two points there are solutions for which the velocity decreases as the Grashof number increases. Without Lorentz forces, $M = 0$ (dashed line in figure 3*b*), u is a monotonic nonlinear function of Gr and u increases with n as buoyancy increases (see figure 3*a*).

An explanation of the triple-valued solution can be given with the help of the acting forces as functions of u. In figure 3(*c*) the sum of the braking friction and Lorentz force $f_v + f_L$ (dashed line) and the driving buoyancy f_b (solid line) for different Gr numbers are given. For $u/|M| > 1$ the friction force gives the dominating

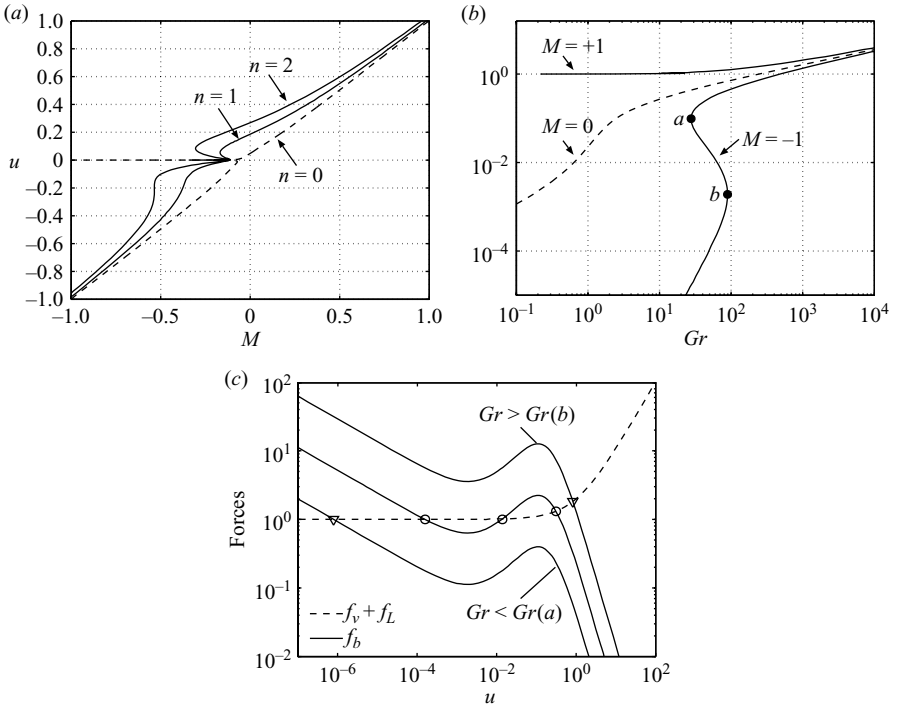

FIGURE 3. The flow characteristics $u(Gr)(a)$ and $u(Gr)(b)$ show the influence of the Lorentz force on a nearly circular loop with $l = 0.005$ and temperature-dependent electrical conductivity. We have chosen the values for $N = 1$ and (a) $Gr = 10$, (b) $n = 2$. For counteracting Lorentz force, $M < 0$, multiple-valued solutions can be observed. (c) The intersection points of the driving buoyancy force f_b (—) and the braking forces friction and Lorentz $f_v + f_L$ (- - -) with $M = -1$.

contribution to the braking forces $f_v \gg f_L$ with $f_v = u$. For $u/|M| < 1$ we have $f_L = M$ as the Lorentz force dominates, i.e. $f_L \gg f_v$. Interestingly, however, buoyancy $f_b(u)$ turns out to be not a monotonically decreasing function of u. Instead, we find $f_b(u)$ increasing with u for a certain limited range of u. Depending on Gr, which leads to a shifting of the curve $f_b(u)$, we have one or three intersection points, as shown in figure 3(c).

To reveal those parameters with dominant influence upon the characteristics of the buoyancy force, let us study the asymptotic expression of $f_b(u)$ for $u/N \ll 1$. It can be readily verified that this expression is

$$f_b(u) = \left(l\frac{n+1}{u}\right)^{1/(n+1)} \left(\frac{n+1}{n+2}l + \frac{u}{N}\right). \tag{3.1}$$

For $l(n+1)/(n+2) \gg u/N$ we have $f_b \sim u^{-1/(n+1)}$. In this regime the fluid is cooled down to the ambient temperature as soon as it enters the cooling section at $s = l$. Therefore, we have 'hot' fluid in the heating zone and 'cold' fluid in the cooling zone. Buoyancy is mainly determined by the temperature at the outlet of the heating section $\theta(l)$, which scales as $\theta(l) \sim u^{-1/(n+1)}$ for all $u/N \ll 1$ as well. The temperature $\theta(l)$ – and hence the buoyancy – decreases with increasing u as the heat input in the heating zone decreases. As the heat input increases with n due to the stronger dependence

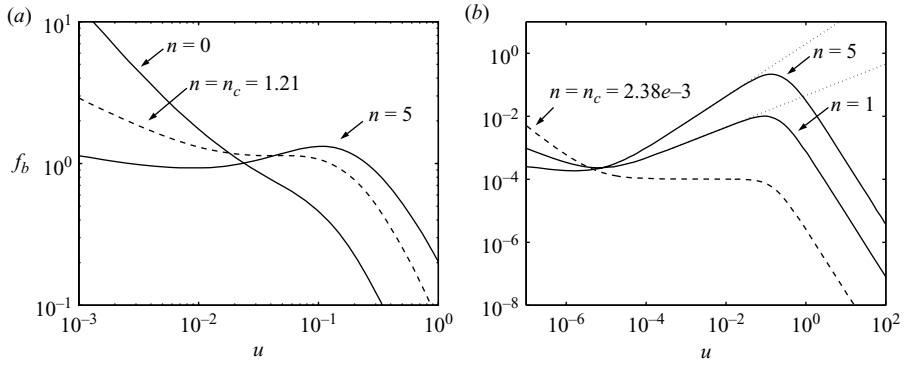

FIGURE 4. The buoyancy force density f_b as a function of the dimensionless velocity u is given for various electrical conductivity parameters n and different lengths of the heating section, namely (*a*) $l = 0.05$ and (*b*) $l = 1e - 5$. For n exceeding a critical value n_c buoyancy increases with u, whereas $n_c \to 0$ for circular loops with $l \to 0$ (in *b*). In this case we find the relation $f_b \sim u^{n/(n+1)}$ for all $n > n_c$ (dotted lines).

of the electrical conductivity on temperature, the function $\theta(l, u)$ – and hence also $f_b(u)$ – flattens with increasing n (see curves in figure 4*a*).

With the increase of u/N, we reach a regime, where the fluid is not cooled to the ambient temperature as soon as it enters the cooling section. We find 'warm' fluid in the upper half-circle of the loop $l \leqslant s \leqslant l + r\pi/2$ which gives an additional contribution to the buoyancy force. Therefore, $f_b(u)$ flattens and the proportionality $f_b \sim u^{-1/(n+1)}$ is left. If we now assume $l \ll 1$, the condition $l(n+1)/(n+2) \ll u/N \ll 1$ is satisfied and (3.1) simplifies to $f_b \approx [l(n+1)/u]^{1/(n+1)} u/N$. For a nearly circular loop we find an increase of buoyancy according to $f_b \sim u^{n/(n+1)}$. In this case the additional buoyancy in the circular arcs is larger than the reduction of buoyancy due to the decrease of $\theta(l)$ with u.

This mechanism of increasing buoyancy is the result of the delicate interplay between (i) temperature-dependent heat input, which is mainly described by n, (ii) the aspect ratio of heating and cooling zones r/l, with $2\pi r + 2l = 1$, which can be described by l, and (iii) the cooling rate, which is described by N. As the buoyancy in the cooling section is proportional to the temperature reduction of $\exp(-N/u)$ and the length of the circular arcs, and $\theta(l) \sim u^{-1/(n+1)}$, the electrical conductivity parameter n needs to exceed a certain critical value n_c for a given N and l. Figure 4(*a*) shows the influence of n on f_b for $l = 0.05$. For $n < n_c = 1.21$ the curve $f_b(u)$ flattens, but $f_b(u)$ does not increase with u. For $n > n_c$ $f_b(u)$ grows with u, but the relation $f_b \sim u^{n/(n+1)}$ is not fulfilled as we do not have $l \ll 1$. The case $l = 1e - 5 \ll 1$, representing a circular loop with $n_c = 2.38e - 3$ (which is virtually zero), is given in figure 4(*b*). The electrical conductivity only needs to depend slightly on temperature and we find an increase of buoyancy. The scaling $f_b \sim u^{n/(n+1)}$ is also fulfilled as indicated by the dotted lines. In general, the smaller the l the smaller the n_c as the influence of buoyancy in the upper circular arcs increases. Besides the increase of buoyancy, we need to have counteracting Lorentz force to obtain multiple solutions. We cannot achieve three intersection points between buoyancy f_b and friction f_v as $f_v \sim u$ and the upper bound for the increase of f_b is $f_b \sim u^{n/(n+1)}$ with $u^{n/(n+1)} < u$. Therefore, the intersection parameter M is an additional parameter which has influence on the onset of the non-unique flow behaviour.

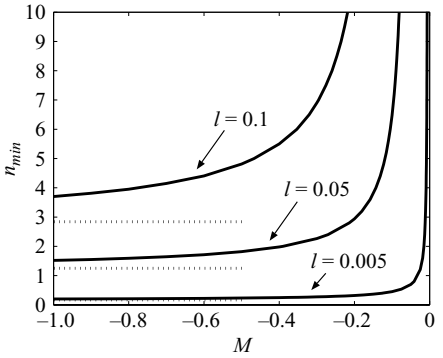

FIGURE 5. The minimum electrical conductivity parameter n_{min} required to give multiple solutions is plotted as function of the interaction parameter M for different values of the length of the heating section l with $N = 1$. The dotted lines indicate n_c for each l.

In order to better understand the parameter dependence of the bifurcations, we have numerically evaluated the smallest electrical conductivity parameter n_{min} that will give rise to multiple solutions as a function of the interaction parameter M for various lengths of the heating section l. The results are shown in figure 5. For $l = 0.1$ a strong nonlinear dependence of the electrical conductivity on temperature and high absolute values of counteracting Lorentz forces $|M|$ are required to achieve non-unique behaviour. In contrast, for a nearly circular loop ($l \to 0$), non-unique solutions can be obtained for small n_{min} and small $|M|$. The dotted lines give the critical value n_c above which buoyancy increases with u. For $M \to -\infty$ the minimum electrical conductivity parameter n_{min} reaches n_c for all values of $l < 0.5$.

3.3. *Temperature-dependent viscosity*

In the present subsection we concentrate our attention on a system with temperature-dependent viscosity which is characterized by the condition $m < 0$. In this case only the structure of the friction force changes from $f_v = u$ for $m = 0$ to $f_v = u f_1(u, N, n, m)$ for $m < 0$ with $f_1 \sim 1 - \exp(-N/u)^m$ (see (2.15)). For about $u/N < 10^{-3}$ the value of $\exp(-N/u)$ is less than the smallest value we can represent with the used code. Therefore, our studies for temperature-dependent viscosity are restricted to $u/N > 10^{-3}$.

If the regime of constant viscosity with $m = 0$ is left, $u(M)$ changes qualitatively as shown in figure 6(a). For moderate m (e.g. $m = -0.2$) there is virtually no difference between the temperature-dependent and the constant viscosity on the lower branch with $u < 0$. By contrast, on the upper stable branch with $u > 0$ we find a turning point such that $u \to 0$ for $M \to +\infty$ and we have four values for u for one M. If the dependence of viscosity on temperature is strong (e.g. $m = -2$), the graph resembles a hyperbola. For a given Gr we need a certain $|M|$ to obtain a solution.

To understand this observation, let us study the mean velocity u as function of Gr for different viscosity parameters m and no Lorentz force ($M = 0$). Figure 6(b) shows that the temperature-dependent viscosity separates the parameter space into three regimes: (i) the freezing regime, (ii) the single-valued regime and (iii) the double-valued regime. The single-valued regime – characterized by a single velocity as solution for a given set of parameters – can only be obtained for a certain Grashof numbers, which we also denote as the critical Grashof number Gr_c. This point in the parameter space forms the overturning point of $u(Gr)$ and marks the onset of

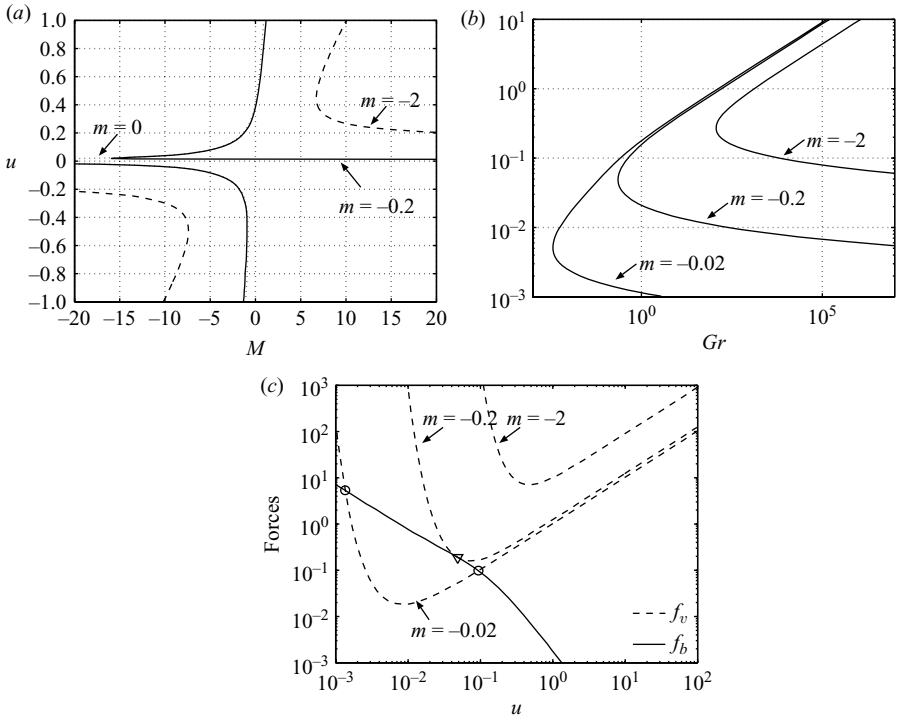

FIGURE 6. The dimensionless velocity u as a function of (a) the interaction parameter M with $Gr = 10$ and (b) the Grashof number Gr for a system without Lorentz force $M = 0$ for different values of the viscosity parameter m with $n = 0$, $N = 1$, $l = 0.25$. (c) The corresponding force distribution for (b) of the the driving buoyancy f_b (—) and braking friction force f_v (- - -) for $Gr = 0.23$ as function of u for different viscosity parameters m. As the friction force has a parabolic-like profile we obtain two (○), one (▽) or no intersection point between f_b and f_v.

convection. If the Grashof number exceeds this critical value, i.e. $Gr > Gr_c$, we reach the double-valued regime and obtain two velocities for one given Gr. Here, for large velocities, u is an increasing function of Gr as it is known from thermal convection. For small velocities, however, u decreases with increasing Gr. For $Gr < \mathrm{Gr_c}$ the model does not give a solution at all. The phase diagram in figure 7 summarizes the region of parameters for all three regimes (i)–(iii).

The reason for the freezing regime is the shape of the friction force given in figure 6(c). For large velocities we have small temperature differences and therefore small viscosity differences within the loop. The friction force is proportional to u. In the case of small velocities the temperature in the cooling zone tends to $\theta \to 0$ and, hence, the viscosity leads to $\eta \to \infty$. Thus, the friction force f_v strongly increases with decreasing u. As a result $f_v(u)$ has a parabola-like shape with a minimum friction force. As the buoyancy curve is monotonically decreasing with u depending on m and Gr, we obtain two, one or no intersection point and therefore two, one or no solution as shown in figure 6(c).

From the two intersection points only the right one is stable and hence, only the upper branch of the two-valued solution is stable. Any u that is slightly above the lower branch will drive the system to the upper stable branch while any u slightly below the lower branch will initiate freezing of the system. Such freezing is not necessarily a contraction. It has been observed for forced convection of glass melt

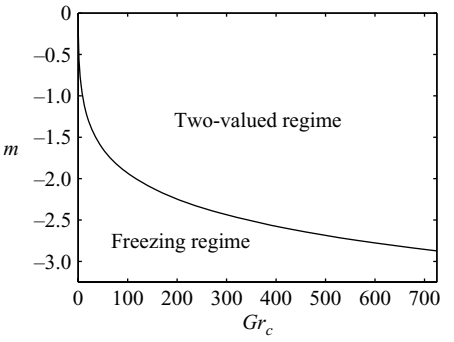

FIGURE 7. The phase diagram gives the region of parameters in which the fluid is immobilized – freezing regime – and in which two solutions do coexist – two-valued regime – for $M = A = 0$, $N = 1$ and $l = 0.25$. Both regimes are separated by the one-valued regime which is characterized by critical Grashof number Gr_c (solid line).

in a pipe in industrial processing and was confirmed theoretically by Lange & Loch (2002) and Giessler, Schlegel & Thess (in press). In practice freezing typically occurs if the melt is cooled by room temperature (for which $\eta \to \infty$) and if the velocity is below a critical value. In a convection cell, a stagnant layer develops and the motion shifts away from the cold walls. In glass processing such a behaviour is used in cold induction crucibles to minimize corrosion at the crucible wall. As the fluid motion in the model is restricted to a defined path, the loop cannot reflect the structural modification of convection cells which is a limit of the thermosyphon approach, in general. However, a second stable branch of $u(Gr)$ (figure 6*a*) exists theoretically. We would be able to calculate this branch, if η would have a finite value for θ_∞. This could be realized for example with the present viscosity law (2.1) and $\theta_\infty > 0$. In this case the friction law $f_v(u)$ would obtain a third branch for $u \to 0$ for which f_v is a linear function of u and one would obtain one to three intersection points.

4. Discussion

4.1. *Summary*

We have presented a one-dimensional model of laminar and steady glass melt flow which we believe to approximate the behaviour of the velocity along a streamline in a convection roll of a glass melt under the influence of external Lorentz force.

We have shown that for a wide range of interaction parameters M, the mean velocity u is a linear function of M. Hence, due to this linearity, the externally imposed Lorentz force can be used to control the velocity easily. Furthermore, we identified regimes for which the solution of u changes from a single-valued one to a multiple-valued one if we switch from pure buoyancy-driven convection to forced convection due to additional external Lorentz force.

In addition, selected results reveal new effects of temperature-dependent material properties on the flow. In the presence of external Lorentz forces the convection of viscous fluids with temperature-dependent electrical conductivity in a circular loop can lead to a novel type of instability. If the dependence of electrical conductivity and the Lorentz force are sufficiently strong, three steady-state solutions can coexist, two of them being stable and one unstable. We also have determined the mechanism that underlies the non-uniqueness. For a viscous fluid with temperature-dependent viscosity we observe three convective regimes: (i) a freezing regime for small Grashof

numbers where the fluid is nearly immobilized, (ii) a single-valued regime, which marks the onset of convection for a certain critical Grashof number $\mathrm{Gr_c}$ and (iii) a double-valued regime for $Gr > \mathrm{Gr_c}$ in which two velocities can be assigned to one Grashof number.

4.2. *Comparison with numerical simulations*

The present analytical loop model was motivated by electromagnetically controlled glass melt flow in a laboratory crucible which was studied experimentally by Hülsenberg *et al.* (2004) and Krieger (2007) and numerically by Giessler & Thess (in press). Here we would like to compare results of the steady three-dimensional simulations with results obtained by the loop model. Before doing this, let us briefly introduce the three-dimensional setup and the adjustment of the model parameters.

Both the experiments by Hülsenberg *et al.* (2004) and the simulations by Giessler & Thess (in press) have been performed for a cylindrical laboratory-scale crucible. The crucible has a diameter of 0.08 m and is filled with molten glass up to a filling height of 0.08 m. Two rod electrodes are symmetrically immersed from above up to 0.06 m into the melt and are supplied by a constant voltage U_0. The super-imposition of the current density in the melt with an externally applied magnetic field density $B_{0,3d}$ leads to a Lorentz force density in the melt. The system is cooled by convection at the crucible walls and by radiation at the free surface. The temperature of the immediate surroundings is controlled to $\theta_\infty = 1393$ K.

The reduction of the three-dimensional setup to the present one-dimensional loop model requires the adjustment of the loop geometry parameter l, r and d, as well as J_0, B_0 and h. A detailed description of the adjustment is given in Giessler (2008). We have performed the calculations with the following loop geometry parameters: length of the heating zone $l = 0.04$ m, arc radius $r = 0.02$ m and inner diameter of the pipe $d = 0.02$ m. Furthermore, we use a current density of $J_0 = 915.5\ \mathrm{A\,m^{-2}}$ which corresponds to $U_0 = 15$ V in the numerical simulation. In the three-dimensional setup the Lorentz force acts in the whole volume of the melt whereas it acts only in the heating zone of our simplified loop model. Taking into account the geometrical ratio l/r, we use a magnetic flux density, henceforth denoted as $B_{0,1d}$, given by $B_{0,1d} = 7.68 B_{0,3d}$. Furthermore, the heat transfer coefficient h is set to $77\ \mathrm{W\,m^{-2}K^{-1}}$ as it approximates the heat transfer by convection at the crucible walls and radiation at the free surface of the melt. For the material property laws we have chosen the following equations:

$$\eta(\theta) = 18.42[\mathrm{Pa \cdot s}]\,(\theta[\mathrm{K}])^{-0.635}, \tag{4.1}$$

$$\sigma(\theta) = 2.3 \times 10^{-3}[\mathrm{S\,m^{-1}}]\,(\theta[\mathrm{K}])^{1.472}, \tag{4.2}$$

with θ being the offset temperature of the system. The numerical simulations are performed with the common exponential formulations for $\eta(\theta)$ and $\sigma(\theta)$. A comparison of both formulations is given in figure 8. For $\theta \to \theta_\infty$ the experimentally measured material properties have a finite, non-zero magnitude which is a large deviation to the power-law formulations of the present model. In this case the analytical model leads to an overestimation of the friction force, which is breaking the flow. At the same time $\sigma \to 0$ results in an overestimation of the heat input and hence, an overestimation of the driving buoyancy force. Without performing detailed calculations we can assume that both effects compensate each other and lead to acceptable flow predictions. However, these large deviations are typically limited to a small temperature range of a few Kelvin and strongly depend on n and m.

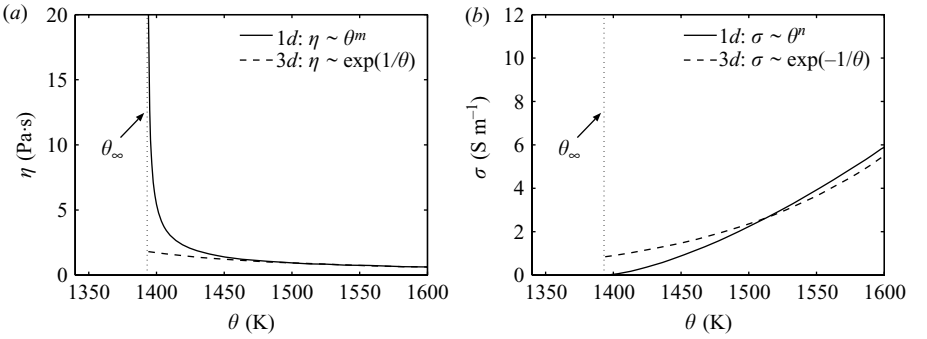

FIGURE 8. Material property laws of (*a*) the viscosity $\eta(\theta)$ and (*b*) the electrical conductivity $\sigma(\theta)$ given in the standard exponential formulation $\eta(\theta) = 9.92 \times 10^{-2}$[Pa·s] exp(1046.20[K]/($\theta$ − 1033.41[K])), $\sigma(\theta) = 1.74 \times 10^{6}$[S m^{-1}] exp(−20 300[K]/θ) and the potential formulation according to (4.1) and (4.2), respectively.

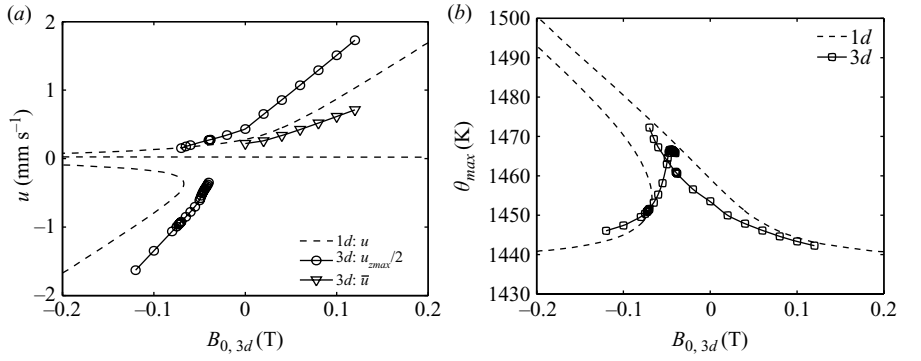

FIGURE 9. Results of three-dimensional numerical simulations compared to results of the 1*d* analytical model obtained with $J_0 = 915.5$ A m^{-2}, $B_{0,1d} = 7.68 B_{0,3d}$, $h = 77$ W m^{-2} K, $l = 0.04$ m, $r = 0.02$ m and $d = 0.02$ m. In (*a*) the velocity u (in mm s^{-1}), and in (*b*) the maximum temperature θ_{max} (in K) as functions of the magnetic flux density of the three-dimensional simulation $B_{0,3d}$ are given. The results of the three-dimensional numerical simulation are given in terms of one half of the maximum z-component of the velocity in the centreline of the crucible $u_{zmax}/2$ and the volume-averaged velocity $\overline{u} = \sqrt{\int |\boldsymbol{u}|^2 \mathrm{d}V / V}$.

Figure 9 summarizes the result of the comparison of our model with the full three-dimensional simulations performed in Giessler & Thess (in press). The calculations for the present model with realistic glass melt parameters involve all the effects which we have studied separately in § 3. The dashed line in figure 9(*a*) gives the mean loop velocity as a function of the magnetic flux density. To compare velocity u of the present model with the velocity of the three-dimensional simulation we use two different quantities, namely $\overline{u}$ and $u_{zmax}/2$. The velocity of the simulation is given in terms of the volume-averaged velocity $\overline{u} = \sqrt{\int |\boldsymbol{u}|^2 \mathrm{d}V / V}$ and the maximum z-component of the velocity in the centreline of the crucible $u_{zmax}/2$. The maximum temperature θ_{max} as function of $B_{0,3d}$ is shown in figure 9(*b*) for both approaches. Overall, the comparison between the results of the analytical loop model and the numerical simulation shows a very good agreement. For $B_{0,3d} \geqslant 0$ the curve $u(B_{0,3d})$ which represents the present model is located in between the numerical curves by $u_{zmax}/2(B_{0,3d})$ and $\overline{u}(B_{0,3d})$. This

indicates that the simplified model is a good approximation to the full problem for the parameter values at hand. The change of the slope of the upper branch during the transition from a driving Lorentz force $B_{0,3d} > 0$ to a breaking one $B_{0,3d} < 0$ is observed for u_{zmax} and for the mean loop velocity u. Also for the clockwise flow with $u < 0$ both approaches are in a very good agreement. Furthermore, we find the multiple-valued regime in the steady numerical simulation which is predicted by the loop model. The transition from a counterclockwise flow with $u_{zmax} > 0$ to a clockwise flow with $u_{zmax} < 0$ results from a relocation and deformation of the convection rolls due to the external Lorentz force. This relocation and deformation cannot be reproduced by the analytical loop model as it represents a convection roll with fixed dimension. Furthermore, in the loop the transition from $u > 0$ to $u < 0$ – characterized by the turning point of the upper branch of $u(B_0)$ – happens due to the temperature-dependent viscosity. As a result, the loop model cannot predict the exact value of $B_{0,3d}$ for which the transition from $u_{zmax} > 0$ to $u_{zmax} < 0$ takes place in the simulation. From the beginning we can exclude a '$\sigma(\theta)$-induced' bifurcation as the dimensionless length is 0.194 and the conductivity parameter is set to $n = 1.472$. To observe that kind of bifurcation n has to exceed a critical value of $n_c = 7.52$.

Also the curves $\theta_{max}(B_{0,3d})$ are in very good agreement (see figure 9*b*) whereas the right branches belong to $u > 0$ and the left branches belong to $u < 0$.

The reader may justifiably ask why the present model is not validated against the experimental results of Hülsenberg *et al.* (2004). The reason for the absence of this comparison is two-fold. First, there is no possibility of velocity measurements in the experiments. Second, a comprehensive comparison of temperature fields is outside the scope of the present paper and is the subject of ongoing work.

4.3. *Outlook*

The present loop model uses a power-law approach according to (2.1) and (2.2) to model temperature-dependent viscosity and electrical conductivity. As the cooling temperature θ_∞ is set to zero, $\eta \to \infty$ and $\sigma \to 0$ for $\theta \to \theta_\infty$. Hence, one has to carefully verify the validity of the loop model for $\theta \to \theta_\infty$. An obvious area of future work would be the implementation of material property law for $\eta(\theta)$ and $\sigma(\theta)$ which would provide finite non-zero values at θ_∞. Vice versa the present potential formulation could lead to finite non-zero values at θ_∞ if the cooling temperature would be greater than zero, $\theta_\infty > 0$. However, to our knowledge it is not possible to find a pure algebraic solution for the loop model, which fulfills this requirements for η and σ and captures the present thermal conditions – direct electrical heating according to the Joule effect in the heating zone and convective heating in the cooling zone. The set of integro-differential equations could only be used by applying a numerical procedure and abandoning goal to achieve an algebraic description.

This work was supported by the Deutsche Forschungsgemeinschaft within the framework of the Forschergruppe 'Magnetofluiddynamik'. We thank D. Hülsenberg, B. Halbedel, U. Lüdtke and U. Krieger for useful discussions.

REFERENCES

Booker, J. R. 1976 Thermal convection with strongly temperature-dependent viscosity. *J. Fluid Mech.* **76** (4), 741–754.

Creveling, H. F., De Paz, J. F., Baladi, J. Y. & Schoenhals, R. J. 1975 Stability characteristics of a single-phase free convection loop. *J. Fluid Mech.* **67** (1), 65–84.

Davidson, P. A. 2001 *An Introduction to Magnetohydrodynamics*. Cambridge University Press.

Desrayaud, G., Fichera, A. & Marcoux, M. 2006 Numerical investigation of natural circulation in a 2d-annular closed-loop thermosyphon. *Intl J. Heat Fluid Flow* **27**, 154–166.

Ehrhard, P. & Müller, U. 1990 Dynamical behaviour of natural convection in a single-phase loop. *J. Fluid Mech.* **217**, 487–518.

Fowler, A. C. 1985 Fast thermoviscous convection. *Stud. Appl. Math.* **72** (3), 189–219.

Ghaddar, N. 1998*a* Analytical model of a side-heated free convection loop placed in a transverse magnetic field. *J. Fluid Engng* **120**, 62–69.

Ghaddar, N. 1998*b* Analytical model of induced electric current from a free convection loop placed in a transverse magnetic field. *Intl J. Heat Mass Transfer* **41** (8–9), 1075–1086.

Giessler, C. 2008 Theoretical investigations of electromagnetic control of glass melt flow. PhD thesis, TU Ilmenau.

Giessler, C., Lange, U. & Thess, A. 2007 Nonlinear laminar pipe flow of fluids with strongly temperature-dependent material properties. *Phys. Fluids* **19**, 043601.

Giessler, C., Schlegel, R. & Thess, A. 2008 Numerical investigation of the flow of a glass melt through along circular pipe. *Intl J. Heat Fluid Flow* **29**(5), 1462–1468.

Giessler, C., Sievert, C., Krieger, U., Halbedel, B., Hülsenberg, D., Lüdke, U. & Thess, A. 2005 A model for electromagnetic control of buoyancy driven convection in glass melts. *Fluid Dyn. Mat. Process.* **1** (3), 247–266.

Giessler, C. & Thess, A. (in press) Numerical simulation of electromagnetically controlled thermal convection of glass melt in a crucible. *Intl J. Heat Mass Transfer*.

Greif, R. 1988 Natural circulation loops. *J. Heat Transfer* **110**, 1243–1258.

Helfrich, K. R. 1995 Thermo-viscous fingering of flow in a thin gap: a model of magma flow in dikes and fissures. *J. Fluid Mech.* **305**, 219–238.

Hofmann, O. R. & Thess, A. 2002 Elektromagnetische Beeinflussung der Glasbadströmung – Ein neues Anwendungsgebiet der Magnetohydrodynamik (in German). *Glas-Ingenieur* **1**, 39–45.

Hülsenberg, D., Halbedel, B., Conrad, G., Thess, A., Kolesnikov, Y. & Lüdtke, U. 2004 Electromagnetic stirring of glass melts using Lorentz forces – experimental results. *Glass Sci. Technol.* **77**, 186–193.

Hülsenberg, D., Halbedel, B., Krieger, U., Schröpfer, D., Thess, A. & Lüdtke, U. 2006 Elektromagnetische Modifizierung von Strömungen in Schmelzen (in German). *Elektrowärme Intl* **2**, 107–110.

Keller, J. B. 1966 Periodic oscillations in a model of thermal convection. *J. Fluid Mech.* **26** (3), 599–606.

Krieger, U. 2007 Einfluss elektromagnetisch generierter Kraftwirkungen auf die strömungen in Glasschmelzen (in German). PhD thesis, TU Ilmenau.

Kunert, C., Langsdorf, A., Lentes, F., Duch, K., Thess, A. & Kolesnikow, Y. 2004 Verfahren und Anordnung zur Zufuhr einer Glasschmelze zu einem Verarbeitungsprozess (in German). DE 10 2004 015 055.

Lange, U. & Loch, H. 2002 Instabilities and stabilization of glass pipe flow. In *Mathematical Simulation in Glass Technology*, Schott Series on Glass and Glass Ceramics (ed. D. Krause & H. Loch). Springer Verlag.

Moresi, L. & Solomatov, V. 1995 Numerical investigation of 2d convection with extremely large viscosity variations. *Phys. Fluids* **7** (9), 2154–2162.

Morris, S. 1996 Stability of thermoviscous Hele–Shaw flow. *J. Fluid Mech.* **308**, 111–128.

Morris, S. & Canright, D. 1984 A boundary-layer analysis of Benard convection in a fluid of strongly temperature-dependent viscosity. *Phys. Earth Planet. Inter.* **36**, 355–373.

Ockendon, H. & Ockendon, J. R. 1977 Variable-viscosity flows in heated and cooled channels. *J. Fluid Mech.* **83** (1), 177–190.

Ogawa, M., Schubert, G. & Zebib, A. 1991 Numerical simulations of three-dimensional thermal convection in a fluid with strongly temperature-dependent viscosity. *J. Fluid Mech.* **233**, 299–328.

Osmanis, A. D., Snijedze, A. K. & Aglitis, A. M. 1987 Influence of electromagnetic stirring of glass melts (in Russian). In *Proceedings of the 12th Riga Symposium on Magnetohydrodynamics*, Salaspils, USSR, pp. 179–183.

Poddubnaya, L. G. & Shaidurov, G. F. 1969 Convective stability of a conducting fluid in a closed circuit. *Magnetohydrodynamics* **5** (2), 63–66.

Richardson, S. M. 1986 Injection moulding of theroplastics: freezing of variable-viscosity fluids. iii. Fully-developed flows. *Rheol. Acta* **25**, 372–379.

Richter, F. M., Nataf, H.-C. & Daly, S. F. 1983 Heat transfer and horizontally averaged temperature of convection with large viscosity variations. *J. Fluid Mech.* **129**, 173–192.

Torrance, K. E. & Turcotte, D. L. 1971 Thermal convection with large viscosity variation. *J. Fluid Mech.* **47** (1), 113–125.

Vogel, W. 1992 *Glaschemie* (in German). Springer.

Welander, P. 1967 On the oscillatory instability of a differentially heated fluid loop. *J. Fluid Mech.* **29** (1), 17–30.

Wylie, J. J. & Lister, J. R. 1995 The effects of temperature-dependent viscosity on flow in a cooled channel with application to basaltic fissure eruption. *J. Fluid Mech.* **305**, 239–261.

Zvirin, Y. 1981 A review on natural circulation loops in pressurized water reactors and other systems. *Nucl. Engng Des.* **67**, 203–225.